

Modulated waves in Taylor–Couette flow

Part 2. Numerical simulation

By K. T. COUGHLIN AND P. S. MARCUS

Department of Mechanical Engineering, University of California at Berkeley,
Berkeley, CA 94720, USA

(Received 2 November 1990)

In part 1 (Coughlin & Marcus 1992*a*) we described the mathematics of temporally quasi-periodic fluid flows, with application to the flow between concentric cylinders (Taylor–Couette flow). In this paper we present numerical simulations of Taylor–Couette flow, motivated by laboratory experiments which show that periodic rotating waves become unstable to quasi-periodic modulated waves as the Reynolds number is increased. We find that several branches of quasi-periodic solutions exist, and not all of them occur as direct bifurcations from rotating waves. We compute solutions to the Navier–Stokes equations for both rotating waves and two branches of modulated waves; those discussed by Gorman & Swinney (1979, 1982), and those discovered by Zhang & Swinney (1985). A simple physical process is associated with both types of modulation. In the rotating frame the quasi-periodic disturbance field (defined as the total flow minus the time-averaged, steady-state piece) appears as a set of compact, coherent vortices confined almost entirely to the outflow jet region. They are advected (with some distortion) in the azimuthal direction along the outflow between adjacent Taylor vortices, with the frequency of modulation directly related to the mean drift speed. The azimuthal wavelength of the disturbance field determines the second wavenumber. We argue that the quasi-periodic flow arises as an instability of the essentially axisymmetric vortex outflow jet. Experimentally, modulated waves appear to bifurcate directly to low-dimensional chaos. Neither the mathematical nor the physical mechanisms of this transition have been well understood. Our numerical work suggests that the observed transition to chaos results from the existence of physically distinct Floquet modes arising from instability of the outflow jet.

1. Introduction

In Part 1 (Coughlin & Marcus 1992*a*) we presented a mathematical description of quasi-periodic solutions to the Navier–Stokes equations in rotating flows with circular symmetry. Generically, rotating waves, which are periodic in the inertial frame but steady in the proper rotating frame, bifurcate to quasi-periodic flows which have two incommensurate temporal frequencies in an arbitrary frame, but are periodic in the correct rotating frame (Rand 1982). Such flows occur in the Taylor–Couette system, in which fluid is confined between a pair of parallel, differentially rotating concentric cylinders. Having long been considered a paradigm problem in the study of laminar and turbulent transitions in fluid dynamics, Taylor–Couette flow provides examples of both rotating waves (referred to as wavy Taylor vortex flow or WVF), and several qualitatively distinct quasi-periodic flows (modulated wavy vortex flow or MWV). (We use the notation developed in

Andereck, Liu & Swinney 1986). In this paper we use numerical simulation to investigate the physical and fluid dynamic character of two quasi-periodic Taylor–Couette flows previously observed in the laboratory; the ‘two-travelling-wave’ flows studied by Gorman & Swinney (1979, 1982) and Shaw *et al.* (1985), which we refer to as GS flows, and the ‘non-travelling modulation’ discovered by Zhang & Swinney (1985), which we term ZS flows. We note that the phenomenology observed in Taylor–Couette flow can be strongly dependent on the geometry of the apparatus (Mullin & Benjamin 1980); hence we have restricted our study to parameters relevant to these experiments.

Our motivation is two-fold: first, experiments on the ZS and GS flows have left open a number of questions, such as how two travelling waves can coexist in a strongly nonlinear flow, or why one should find both non-travelling and travelling modulations; secondly, we believe this problem can shed light on the transition to chaos in this system, and in general to the application of ideas about low-dimensional chaos to fluids. Although a number of experiments on fluids have demonstrated that the quantitative signatures of low-dimensional chaotic attractors can be constructed from laboratory data (see Abraham, Gollub & Swinney 1984), the exact nature of the dynamical degrees of freedom in such systems often remains obscure. Quasi-periodic flows, while not chaotic, are also flows with non-trivial dynamics that are described by low-dimensional attractors (specifically, two-tori for MWV) in an infinite dimensional phase space; hence, they can be used to investigate in detail the relation between the fluid motion and the mathematical representation of the solution. Therefore, we use detailed simulation to construct simple descriptions of the flows in such a way that the temporal degrees of freedom are connected with physical behaviour.

Our initial-value code (Marcus 1984*a*) finds stable, three-dimensional, time-dependent solutions to the Navier–Stokes equations for imposed values of the axial and azimuthal periodicity. By defining the quasi-periodic component of the flow as the total velocity minus its time-averaged value in the proper rotating frame, we are able to present an explicit picture of the fluid motion associated with the modulation, which leads to a direct identification of the parameters appearing in the formal solution derived in Part 1. We show that while ZS and GS flows are both instabilities of the outflow jet between adjacent Taylor vortices, different characteristics of the Floquet modes lead to different experimental signatures. We discuss the instability of the outflow jet in the framework of the overall development of the flow as the Reynolds number $R \equiv \Omega a(b-a)/\nu$ increases, where Ω is the inner cylinder frequency, ν the kinematic viscosity, and a and b the inner and outer cylinder radii respectively. In our conclusions we discuss the relation between this work and the experimentally observed transition to chaos.

In Part 1 we review the ‘main sequence’ of transitions in Taylor–Couette flow (Golubitsky & Stewart 1986), which we summarize briefly here: When the outer cylinder is held fixed and the gap width is small (here $\eta \equiv a/b = 0.875$), as the inner cylinder speed is increased the flow passes through a sequence of laminar states, beginning with circular Couette flow. At $R \equiv R_c$ there is a bifurcation to axially periodic, axisymmetric Taylor vortex flow (TVF). A supercritical Hopf bifurcation leads to WVF which consists of azimuthally travelling waves on the vortices. At still higher R the periodic flow becomes modulated, with the power spectrum characterized by the presence of two incommensurate frequencies. The flow is quasi-periodic relative to the laboratory frame, but periodic in the frame rotating with the original travelling wave (we will refer to the latter as the underlying wave). The

azimuthal wavelength of the flow may change in this transition, so the new flow must be described not only by two temporal frequencies but also by two azimuthal wavenumbers (the axial periodicity does not change). As R is further increased, a broad peak appears in the power spectrum and there is a rise in the background noise level (Gollub & Swinney 1975; Fenstermacher, Swinney & Gollub 1979); thus, modulated waves appear to bifurcate directly to low-dimensional chaos. The exact mechanism of this transition is not well understood. For a wide range of R beyond the transition to chaos the basic Taylor vortex structure remains in place, with the flow marked by disordered small-scale structure; hence the designation of the flow as chaotic rather than turbulent. Experimentally, it has been shown that the dynamics of the chaotic flow can be described by a low-dimensional strange attractor (Brandstater *et al.* 1983, Brandstater & Swinney 1987).

In Part 1 we showed that the azimuthal wavenumber and frequency of modulation are mathematically well-defined. At the onset of MWV, the modulation is due to a Floquet mode with positive growth rate. Nonlinear MWV can be written as a non-separable function of the two phases $m_1(\theta - c_1 t)$, $m_2(\theta - c_2 t)$, where m_1 and m_2 are the azimuthal wave numbers, and c_1 and c_2 the phase speeds of the rotating wave and Floquet mode respectively. The different types of modulation observed experimentally are easily characterized by different numerical values of c_2/c_1 (which are approximately independent of R , m_1 and m_2), the spectral amplitudes of the solution, and the spatial character of the modulation. A discussion of the relevant experimental work appears in Part 1.

The existence of multiple branches of quasi-periodic solutions does not in itself contradict the main sequence scenario, which is essentially a description of the symmetry-breakings that may occur sequentially in this flow. However, numerical and experimental work has shown that other sequences of bifurcations are common. For example, the direction of bifurcation can reverse with R (even at low values of R/R_c), and one may see transitions from WVF to TVF as R increases (Park 1984), from a chaotic flow to MWV, or from a ZS to a GS flow. The latter transition was predicted by the numerical simulations described here, and subsequently verified in the laboratory (Coughlin *et al.* 1991). The actual physics governing transition is thus dependent in a complicated way on the base flow, and there is no ‘universal’ transition from WVF to MWV. With this in mind, we concentrate in this paper on presenting a description of the flows themselves, focusing on understanding why the unstable flow features lead to modulated waves with the particular structure they have.

The outline of the rest of the paper is as follows: in §2 we define our numerical problem. The code itself has been discussed in Marcus (1984*a*) and a description of our numerical diagnostics appears in the Appendix to Part 1. In §3 we present numerical results for both ZS and GS modulated waves, illustrating the basic structure and temporal behaviour of the modulation. In §4 we discuss the flow features which generate the instability, drawing on numerical computations of WVF over a large range of Reynolds number. Our discussion, and the implications of our work for the understanding of low-dimensional chaos in this system, are presented in §5.

2. Numerical problem

We use a pseudo-spectral initial-value code to solve the Navier–Stokes equations for incompressible flow in a cylindrical geometry. Experimentally, the geometry of

the apparatus is characterized by the radius ratio η and the aspect ratio Γ which is equal to the height of the fluid column divided by the gap width. In this paper (and in Part 1) we assume exact periodicity in the axial direction. In Taylor–Couette flow, axial end effects include both secondary circulation due to the presence of physical boundaries and the $O(1)$ symmetry breaking in the axial direction. Because of this symmetry breaking, the transition to Taylor vortex flow is an imperfect bifurcation which establishes approximate periodicity in the interior of the apparatus. Small non-uniformities in the axial wavelength of the vortices are confined primarily to the end cells (Park, Crawford & Donnelly 1981; King 1983; Dinar & Keller 1985). In the infinite cylinder model, transition to TVF breaks the continuous axial symmetry and establishes perfect axial periodicity. In subsequent bifurcations, the symmetries which are broken (axisymmetry, time independence) are well-realized in the laboratory apparatus; hence they can be treated to a very good approximation under the assumption of axial periodicity. Studies have shown that there is some dependence on the aspect ratio of the critical Reynolds number for onset of both the rotating wave and modulated wave flows, however, these do not affect the nature of the final flow state if the radius ratio is fixed and the aspect ratio is large enough (Cole 1976; King & Swinney 1983; Mullin 1985; Ross & Hussain 1987). The real test of the validity of these assumptions is comparison with experimental work. Previously, our code was used to compare wave speeds in WVF to laboratory measurements and found to agree within 0.1%, with very little aspect ratio dependence (King *et al.* 1982; Marcus 1984*b*). For our computations of both ZS and GS modes in experimentally accessible parameter ranges, the agreement with measured modulation periods is within 6% (Coughlin *et al.* 1991; see also table 2 of Part 1).

A more severe restriction in the theoretical work is the imposition of fixed wavelengths in the axial and azimuthal directions, which prohibits the wavelength changing transitions commonly seen in the laboratory. In Taylor–Couette experiments modulated waves are often observed to bifurcate from rotating waves without any change in these wavelengths, therefore we assume that the relevant physics can be captured with these parameters fixed. (We point out, however, that the transition sequences observed for fixed axial and azimuthal wavelength can be sensitive to the actual values imposed (Coughlin 1990).)

We describe the flow in terms of the usual cylindrical coordinates (r, θ, z) . Our non-dimensionalization sets the gap width $(b - a)$, the inner cylinder velocity Ωa , and the density all equal to one. We define λ as the axial and $2\pi/s$ as the azimuthal wavelength. In this work we set $m_1 \equiv s$ with $s \geq 4$; hence we force $m_2 = js$ for integer j . We have observed flows with both $j = 1$ and $j \neq 1$. In the discussion below we will not refer to c_2 as a wave speed; any reference to a wave speed implies c_1 . We will use the notation $\text{ZS}(m_1, m_2)$ to denote a ZS modulated with azimuthal wavenumbers m_1 for the underlying WVF and m_2 for the Floquet mode, and similarly for $\text{GS}(m_1, m_2)$.

We place an additional restriction on the flow by imposing shift-and-reflect symmetry (Marcus 1984*a, b*). With the proper choice of origin in z , under

$$(r, \theta, z) \rightarrow (r, \theta + \pi/s, -z), \quad (1)$$

the velocity transforms as

$$(v_r, v_\theta, v_z) \rightarrow (v_r, v_\theta, -v_z), \quad (2)$$

and the vorticity as

$$(\omega_r, \omega_\theta, \omega_z) \rightarrow (-\omega_r, -\omega_\theta, \omega_z). \quad (3)$$

This reduces the number of Fourier modes needed to represent the flow by a factor of two. Any modulated wave with m_2/m_1 equal to an integer can have this symmetry.

We have tested several MWV flows for stability to non-shift-and-reflect perturbations, which in all cases decay on a timescale comparable to the modulation period. Many of the flows computed with shift-and-reflect symmetry have been observed in the laboratory, implying that any breaking of this symmetry is small and not relevant to the problem at hand. We have attempted, with R, λ, s and η held fixed, to find MWV final states with different values of m_2 and c_2 by varying the initial conditions, but find that the flow always converges to a unique final state.

To describe the temporal properties of the modulation we shall use both the phase speed c_2 of the Floquet mode and the modulation frequency ω_M (see (11) in Part 1). The latter is defined as the modulation frequency observed in a frame rotating with the speed c_1 of the underlying wave, and can be directly compared to experimentally measured values. The modulation period $T_M \equiv 2\pi/\omega_M$ is the periodicity observed in this frame, measured in our dimensionless units.

All figures of the velocity and vorticity are presented with respect to the frame rotating with angular velocity c_1 . We define the mean flow \bar{v} to be the time-averaged piece of the velocity in the frame c_1 , and the quasi-periodic component v_{qp} to be $v - \bar{v}$. With this definition, near onset of the modulation, \bar{v} is equal to the unstable WVF, and v_{qp} is the Floquet mode. For reference, the precise definitions are (see Part 1):

$$\bar{v}(r, \hat{\theta}, z) \equiv \frac{1}{T_M} \int_0^{T_M} v(r, \hat{\theta}, z, t) dt, \quad (4)$$

$$\text{and} \quad v_{qp}(r, \hat{\theta}, z, t) \equiv v(r, \hat{\theta}, z, t) - \bar{v}(r, \hat{\theta}, z), \quad (5)$$

where $\hat{\theta} \equiv \theta - c_1 t$. Note that \bar{v} always has the symmetry of the underlying wave. Our convention is to choose the phase in z so that shift-and-reflect symmetry is satisfied and the outflow jet of the axisymmetric component of the flow is at $z = \frac{1}{2}\lambda$. We scale the inner cylinder speed $\Omega a \equiv 1$, so an increase in R corresponds to a decrease in the viscous dissipation. With this scaling, the magnitude of v_θ is of order unity, and the magnitudes of v_r and v_z are of order 10^{-1} , approximately independent of R .

3. Numerical results

In this section we present detailed numerical results for both the ZS and GS modulated waves for two sets of parameters; $\lambda = 3.0$, $s = 6$, $2.1R_c \leq R \leq 9R_c$ and $\lambda = 2.5$, $s = 4$, $8.5R_c \leq R \leq 10R_c$. These include examples of both $m_1 = m_2 = s$ and $m_1 \neq m_2$. We have observed no significant dependence of the detailed flow structure on the axial or azimuthal wavelengths. For one of the ZS flows ($\lambda = 3.0$, $s = 6$), we find that the transition occurs as a supercritical Hopf bifurcation directly out of WVF, with the amplitude of modulation scaling as $(R - R_M)^{\frac{1}{2}}$ and the frequency as $R - R_M$, where $R_M = 6.7R_c$ is the critical value for onset of quasi-periodicity. The data are presented in table 1. For the other ZS mode and the GS mode, as R is decreased the flow does not return to a WVF state, but rather becomes temporally disordered. Thus, not all MWV flows bifurcate directly out of WVF.

Our criteria for distinguishing ZS modes are (i) the ratio of phase speeds c_2/c_1 , or equivalently the period of the modulation relative to $2\pi/(m_1 c_1)$, (ii) the characteristic strength of modulation, and (iii) the spatial structure of the modulation. We make use of experimental modulation frequencies and spatial information whenever it is available to corroborate our results. For GS modes, $c_2/c_1 \approx \frac{4}{3}$ in agreement with the data of Shaw *et al.* For ZS modes, $c_2/c_1 \approx 2$, which we have shown in Part 1 to be consistent with the spectral data of Zhang & Swinney. The modulation amplitude for

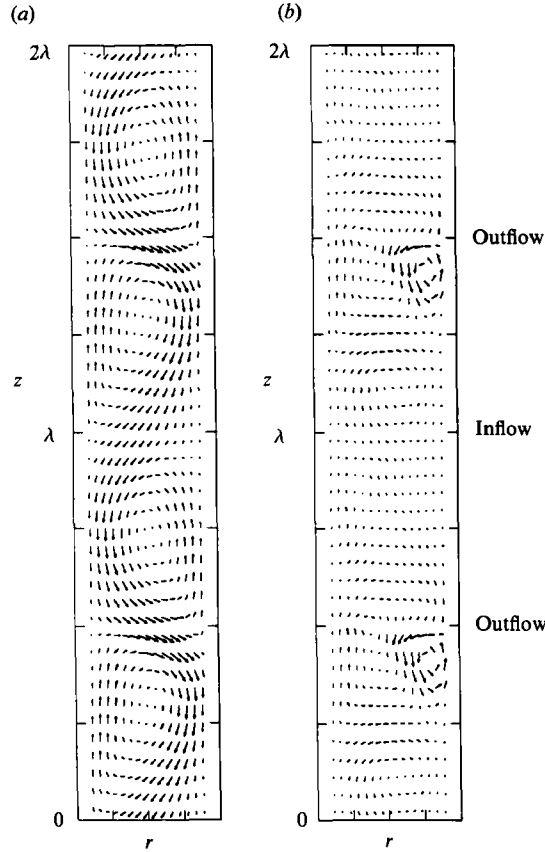


FIGURE 1. (a) Total flow and (b) v_{ap} for a ZS (6, 6) with $\lambda = 3$, $R = 8R_c$. The velocities are projected onto an (r, z) -plane at fixed θ and t in the frame rotating with speed c_1 . (Note: for projections onto this plane, the inner cylinder is always on the left.) The outflow is at $z = \frac{1}{2}\lambda$. Two wavelengths in z are plotted.

R/R_c	ϵ	$\epsilon/(R - R_M)^{\frac{1}{2}}$	ω_M
6.5	0	0	0.2976
7.0	0.030	0.055	0.2962
7.5	0.049	0.055	0.2948
8.0	0.063	0.057	0.2935

TABLE 1. Amplitude ϵ and frequency ω_M for the Hopf bifurcation to a ZS mode with $\lambda = 3.0$, $s = 6$ and $R_M = 6.7R_c$

GS modes is larger (in a sense to be defined precisely below) than for ZS modes, but both are weak compared to the amplitude of the rotating wave.

3.1. ZS modulated waves

For $\lambda = 3.0$, $s = 6$ a stable WVF exists at $R = 6.5R_c$. To begin a computation with a new value of R , we use as the initial condition a converged solution for a value of R about 10 % lower. This procedure leads to transients dominated by the most slowly decaying eigenmode of the stable flow at the current value of R , or if the initial condition is unstable, by the most rapidly growing eigenmode. At $R = 6.5R_c$, the

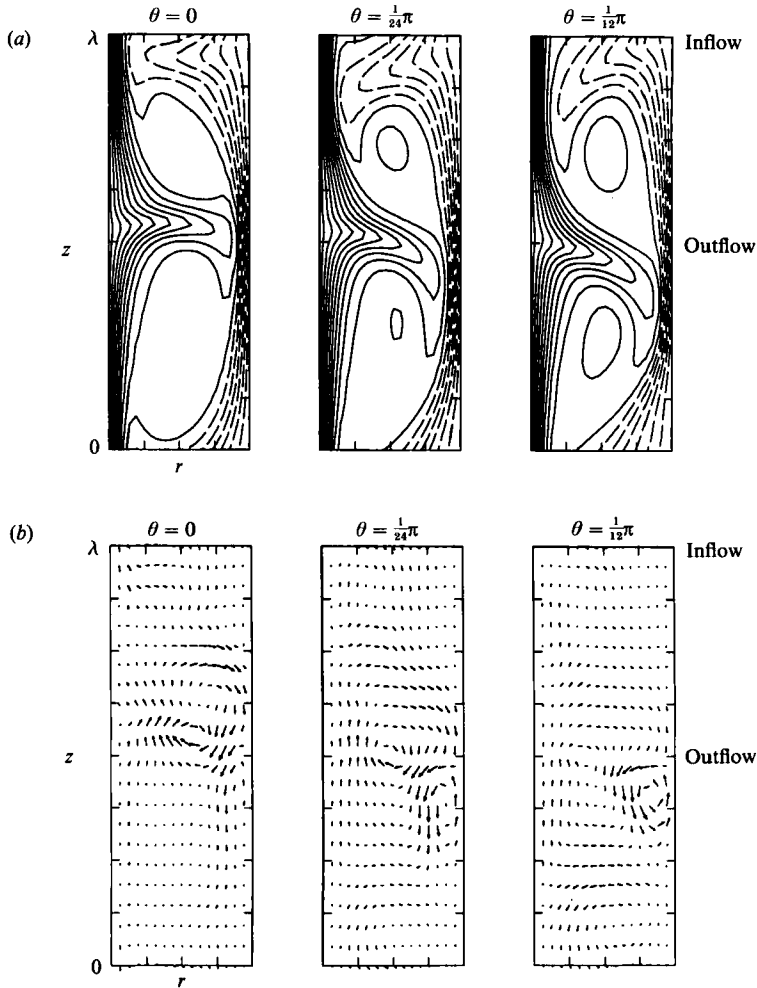


FIGURE 2. (a) Contours of constant v_θ plotted in a set of (r, z) -planes at fixed time for the flow in figure 1. (Note: for all contour plots, solid contours represent positive values and negative values are shown by long-dashed contours.) (b) Projections of the quasi-periodic piece of the flow onto the same set of (r, z) -planes.

transients are dominated by a very slowly decaying modulation with a frequency identified as ω_M in table 1. At $R = 7R_c$ the flow is supercritical, with a slowly growing modulation that eventually saturates to an MWV equilibrium. In both cases, the modulation frequency ω_M converges to a constant value within a few modulation periods. Near the critical R_M , there is a single strong peak in the temporal power spectra calculated with respect to the c_1 -frame, verifying that the instability is a Floquet mode.

We illustrate the structure of the flow in figure 1, which shows a projection onto an (r, z) -plane at fixed θ and t of a ZS(6, 6) flow at $R = 8R_c$. In figure 1(a) we plot the total field, showing the basic Taylor vortex structure modified by the wave, the latter appearing as an axial flow across the radial inflow (near $z = 0$) and outflow (near $z = \frac{1}{2}\lambda$). Note that, in this projection, there is no visually identifiable difference between this flow and a stable WVF at $R = 6.5R_c$. In figure 1(b), we plot the quasi-periodic disturbance v_{qp} , which is representative of the Floquet mode at onset. The

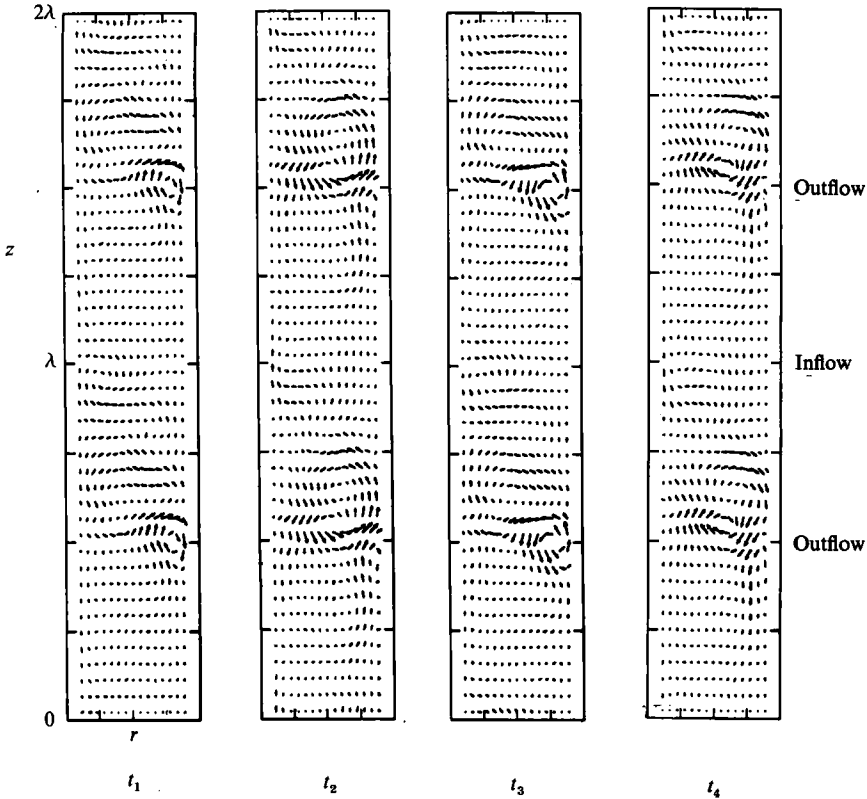


FIGURE 3. Projections of the quasi-periodic piece of the flow in figure 1 onto an (r, z) -plane at fixed $\theta = 0$, at four equally spaced times in the modulation period. Two wavelengths in z are plotted.

quasi-periodic disturbance is confined to the region near the outflow of the total flow, not just at this point but for all θ and t . It has the shape of a small vortex in the (r, z) -plane, which is of positive sign over one half of the azimuthal wavelength, and negative over the other half (by shift-and-reflect symmetry.) Outside this vortex v_{qp} is almost zero.

The axial location of the disturbance vortex v_{qp} as a function of θ is directly correlated with the location of the outflow jet of the total flow. We illustrate this feature in figure 2 (see also figure 9). In figure 2(a) we plot contours of the total azimuthal velocity in an (r, z) -plane at three locations in θ relative to the c_1 -frame. Here, the outflow (inflow) boundaries appear as azimuthal jets of relatively high-(low-) speed fluid extending into the interior of the gap. In figure 2(b), v_{qp} is projected as in figure 1(b), and it is clear that its axial location changes as a function of θ to follow the location of the outflow.

The temporal behaviour of v_{qp} , at fixed θ , is shown in figure 3 where the quasi-periodic field in an (r, z) -plane is plotted at the four equally spaced times $t_j = jT_M/4$, $j = 1, 2, 3, 4$. The energy of the total flow is a maximum at t_1 , and a minimum at t_3 . The quasi-periodic vorticity is advected towards the outer wall by the radial outflow jet, where it is destroyed by the large shear in the radial boundary layers. The disappearance of the vortex of one sign is correlated with the generation of a vortex of the opposite sign in the interior region. The timescale for this process is equal to the modulation period, and is approximately equal to twice the gap-width divided by the mean radial outflow velocity.

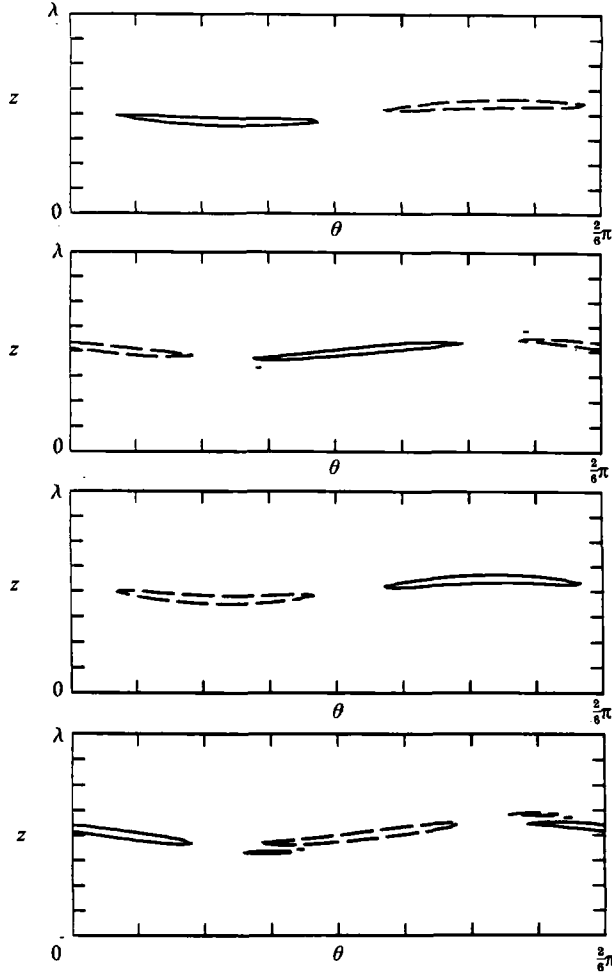


FIGURE 4. Contours of constant azimuthal vorticity for the ZS flow in figure 1, with the quasi-periodic mode plotted in the (θ, z) -plane at mid-gap at four equally spaced times. Only the contour values ± 0.2 are plotted; inside this contour the vorticity increases, and outside drops rapidly to zero (see figure 5).

At onset, the time dependence of the quasi-periodic piece of the flow is given by a single temporal Fourier mode (relative to the c_1 -frame),

$$v_{qp}(r, \hat{\theta}, z) \approx \text{Re} \{ \exp [i(m_2 \hat{\theta} - \omega_M t)] F(r, \hat{\theta}, z) \} \quad (6)$$

and thus is exactly anti-symmetric under $t \rightarrow t + \frac{1}{2}T_M$. The generation of even harmonics of the modulation frequency by the nonlinearities breaks this anti-symmetry, but owing to the relative weakness of higher temporal harmonics it remains approximately valid. For the flow illustrated in figures 1 and 2, $m_2 = m_1$ and v_{qp} is shift-and-reflect symmetric, so a spatial translation of the azimuthal vorticity through $\theta \rightarrow \theta + \pi/m_2$ is approximately equivalent to a time translation by $\frac{1}{2}T_M$ and reflection through $z = \frac{1}{2}\lambda$ (the equivalence is exact at onset). Thus, the time dependence of the disturbance is approximated by advection at a speed equal to the azimuthal wavelength of v_{qp} divided by the modulation period.

This advection of v_{qp} is clearly illustrated in figure 4. Here we show contour plots of the θ component of the quasi-periodic vorticity ($\nabla \times v_{qp}$), projected onto the (θ, z) -

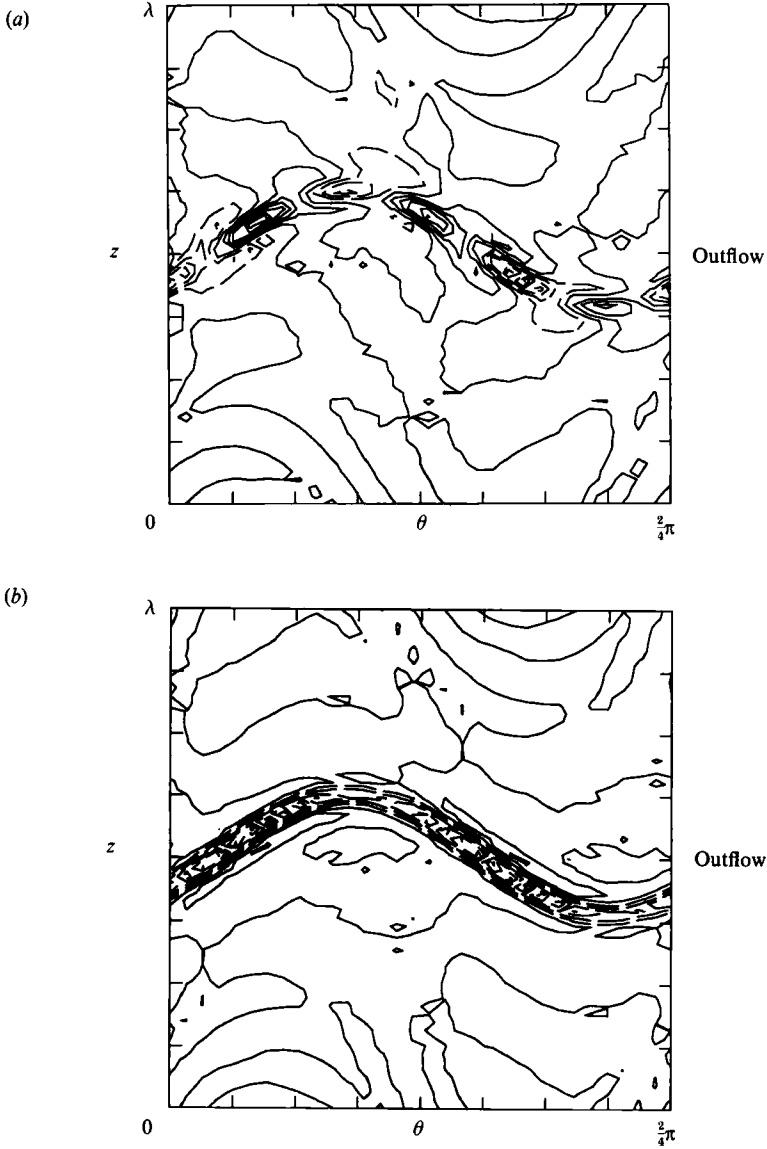


FIGURE 5. Azimuthal vorticity plotted in the (θ, z) -plane, for $\lambda = 3$, $s = 4$, $R = 7.5R_c$. The vertical direction is stretched to clarify the structure of the flow. (a) The vorticity of the quasi-periodic piece of the flow, which is approximately equal to the Floquet mode Q_F . For this flow $m_2 = 3s$, as can be seen from the number of vortex pairs of opposite sign per wavelength $2\pi/s$. The contour interval is 0.05. (b) Vorticity of the Floquet eigenfunction. This eigenfunction is constructed by computing $\exp[-im_2(\theta - c_d t)] Q_F(r, \theta, z, t)$, where Q_F is the Floquet mode (see (7) of Part 1). We plot the real part, which for this choice of origin in t is approximately five times as large as the imaginary part.

plane at mid-gap ($r = \frac{1}{2}(a + b)$). Each figure represents the flow at one of the four equally spaced times t_j . For clarity only two contour values have been plotted – the vorticity increases in absolute value inside the contour, and outside drops rapidly to zero (see also figure 5). Solid contours represent positive values of the vorticity, dashed contours represent negative. The quasi-periodic piece of the flow consists of a pair of three-dimensional vortices which drift azimuthally along the outflow contour at an average speed c_d (defined below in (7)). There is only one vortex pair

λ	m_1	m_2	R/R_c	c_1/Ω	T_M	c_2/c_1	Flow
2.5	4	12	8.5	0.3380	10.6	2.02	ZS
3.0	4	12	7.5	0.3340	11.1	2.03	ZS
3.0	5	5	7.5	0.3526	22.1	2.13	ZS
3.0	6	—	6.5	0.3568	—	—	WVF
3.0	6	6	8.0	0.3709	21.4	1.92	ZS

TABLE 2. Modulation periods T_M and phase speeds for ZS modulated waves

per wavelength of the underlying wave, consistent with the identification $m_2 = m_1$. This should be compared with the plot in figure 5(a) of $\hat{e}_\theta \cdot (\nabla \times \mathbf{v}_{qp})$ for a ZS(4, 12) mode. In this case, there are three pairs of plus/minus vortices spaced along the outflow, implying that $m_2 = 3m_1$, which is confirmed by the structure of the azimuthal Fourier spectrum of the quasi-periodic flow presented in the Appendix to Part 1. Note also that the quasi-periodic disturbance field is truly concentrated entirely at the outflow jet, and that there is no symmetry of \mathbf{v}_{qp} under the transformation $\theta \rightarrow \theta + 2\pi/m_2$.

The temporal behaviour of \mathbf{v}_{qp} for all the ZS modes is as follows. In one period T_M a single vortex pair drifts over one ‘wavelength’ of the modulation $2\pi/m_2$, thus the logical definition of the drift speed is

$$c_d \equiv \frac{2\pi}{m_2 T_M}. \quad (7)$$

Thus $c_d = \omega_M/m_2$. With the definition $c_2 = c_1 + \omega_M/m_2$ from Part 1, we may rewrite

$$c_2 = c_d + c_1. \quad (8)$$

The phase speed c_2 is just the drift speed of the quasi-periodic vorticity relative to the inertial frame. It is important to note that advection of \mathbf{v}_{qp} is approximate – it is accompanied by some distortion of the vortices and of the underlying flow. The quasi-periodic disturbance in this frame is not a true travelling wave, as it has neither constant speed nor constant shape as it drifts along. However, it is clear from the plots that the vortices comprising the quasi-periodic disturbance are coherent features, and that the dominant effect is advection by the mean flow. This advection process can be used to determine m_2 graphically, by setting $2\pi/m_2$ equal to the azimuthal distance traversed by one vortex pair in one modulation period (relative to the c_1 frame), which is consistent with the determination from spatial spectra given in Part 1. For all our computed ZS modulated waves the drift speed is approximately constant, with $c_2/c_1 \approx 2$. Some numerical values are listed in table 2.

The structure of the quasi-periodic flow implies, for shift-and-reflect symmetric fields, that m_2/m_1 must be odd (for these cases $m_1 = s$), which is what we find numerically in all cases. As a vortex is advected azimuthally, it remains coherent while its axial location oscillates above and below the symmetry plane at $z = \frac{1}{2}\lambda$. The sign of each vortex remains positive or negative. At onset, the quasi-periodic component of the vorticity is a Floquet mode with θ -component (as observed in the c_1 rotating frame) of the form $\exp[im_2(\hat{\theta} - c_d t)]g(r, \hat{\theta}, z)$. If the flow is s -fold symmetric in θ and has shift-and-reflect symmetry (see (3)), then under $\theta \rightarrow \theta + \pi/s$, $z \rightarrow -z$, this vorticity transforms to $(-1)^{m_2/s} \exp[im_2(\hat{\theta} - c_d t)]g(r, \hat{\theta} + \pi/s, -z)$. Thus if m_2/s is even, g must have odd parity under the shift-and-reflect operation, and if m_2/s is odd, g must have even parity. The Floquet mode for the azimuthal vorticity

has the additional property that if a compact vortex is located a distance δz above the symmetry plane at $z = \frac{1}{2}\lambda$, then after a time π/sc_d it has travelled a distance s/π in θ , is a distance δz below the symmetry plane, and has the same (opposite) sign that it had initially if g has even (odd) parity. Our results show that the vortex travels coherently; its vorticity does not pass through zero and change sign as it advects azimuthally. Hence g must have even parity, and shift-and-reflect symmetry requires that m_2/s be an odd integer. This is illustrated in figure 5(b), where we plot contours of g in the (θ, z) -plane at mid-gap for a ZS mode. Note that shift-and-reflect symmetric Floquet modes with m_2/s even must exist, but do not appear in our numerical calculations; hence they must be decaying modes over the parameter range that we have investigated. If an even m_2/s mode were to grow to equilibrium, the vorticity associated with the modulation would oscillate in sign as it advected azimuthally, and the signature of the flow would look different from a ZS or GS mode.

We have projected all components of the quasi-periodic velocity and vorticity onto the (r, θ) , (θ, z) - and (r, z) -planes, and find in all cases that the disturbance is localized at the outflow jet, with maximal amplitude in regions of large ambient shear. (In these regions the surrounding v_r and v_θ also have local maxima.) Thus, we can confirm that the disturbance is well-characterized as a set of compact, coherent three-dimensional vortices, regardless of how the flow is projected. This is true over the entire range of R in which these modes exist, with the intensity of the disturbance increasing with R but the spatial structure remaining the same. While some aspects of the ZS modes shown so far are specific to these flows, there are three features which we can enumerate as generic for the quasi-periodic disturbance. (i) The quasi-periodic mode consists of pairs of compact, three-dimensional azimuthal vortices of opposite sign, which are localized near the outflow jet of the underlying rotation wave flow. (ii) The timescale of the modulation is related to advection, with some distortion, of the disturbance vorticity by the ambient v_θ . The second phase speed c_2 is non-dispersive and characteristic of a particular kind of modulated wave. (iii) Shift-and-reflect symmetry of the total flow is not broken by the transition to modulated waves if m_2/m_1 is equal to an integer. This integer must be odd. All our examples of modulated waves have these features in common, including the low R flows discussed in Coughlin (1990).

The ZS modes are characterized in addition by the following features: (i) The disturbance vorticity is very highly localized both in r (near the outer cylinder) and z . The axial width of the quasi-periodic vorticity field is equal to the width of the outflow of the underlying wave (see figure 9). (ii) The modulation is small and interacts weakly with the underlying flow, having little effect on the shape of the outflow jet contours. (iii) The drift speed of the quasi-periodic mode is relatively large; $c_2 \approx 2c_1$. The speed c_2 is equal to the azimuthal velocity at a radius near to, but closer to the inner cylinder than, the location of the quasi-periodic disturbance. Experimentally, the ZS modulation is visible as small ripples which travel along the outflow at a speed obviously greater than the wavespeed c_1 (Coughlin *et al.* 1991).

3.2. GS modulated waves

The GS modes share the same basic structure as the ZS flow, as illustrated in the next two figures. In figure 6 we plot a GS(4, 4) mode for $R = 9.8R_c$ and $\lambda = 2.5$, using the same (r, z) projections as in figure 1. Figure 6(a) shows the total velocity, and figure 6(b) the quasi-periodic disturbance. In the latter, the quasi-periodic field is again a single vortex at the outflow, significantly less localized than the ZS mode, both in z

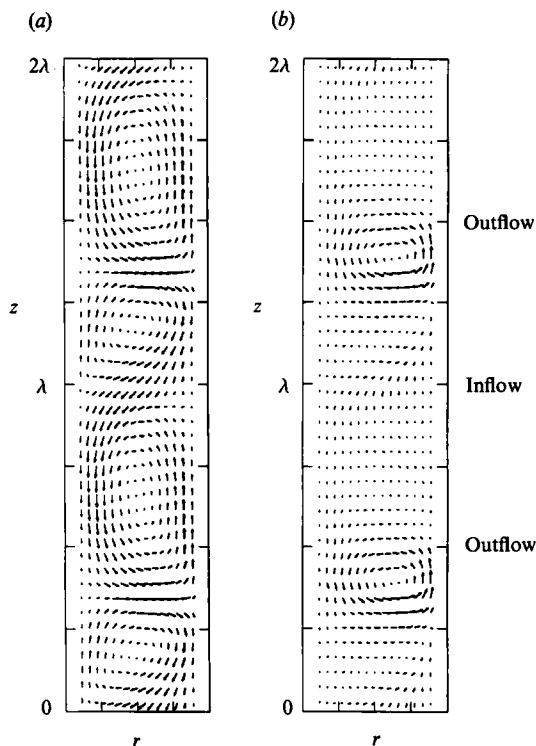


FIGURE 6. (a) Total flow and (b) v_{θ} for a GS mode with $\lambda = 2.5$, $s = 4$, $R = 9.8R_c$. The velocities are projected onto an (r, z) -plane at fixed θ and t in the frame rotating with speed c_1 . The outflow is at $z = \frac{1}{2}\lambda$. Two wavelengths in z are plotted. Compare to figure 1.

and in r . Experimentally, the visual signature of the onset of GS modulation is the periodic flattening of the outflow boundaries of the underlying WVF. For $m_2 = m_1$ the flattening occurs on all m_1 of the azimuthal waves in phase. In figure 7 we plot the θ component of $\nabla \times v_{\text{qp}}$ at four equally spaced times in the modulation. As in figure 4, only two contours are shown, with the magnitude of the vorticity dropping to zero outside this contour and rising to an extremum within. The quasi-periodic vorticity simultaneously drifts in the azimuthal direction and flattens with the outflow of the total flow. The drift speed c_d is defined as it was for the ZS flow, and is approximately equal to $\frac{1}{3}c_1$, which implies that $c_2/c_1 \approx \frac{4}{3}$. Note that this translates into a much longer characteristic period of modulation for the GS modes compared to the ZS modes. For example a GS(m_1, m_1) flow will have a period three times longer than a ZS(m_1, m_1) flow, approximately independent of R , λ and m_1 .

This GS mode does not occur as a bifurcation out of WVF. At $R = 9.25R_c$ the flow is aperiodic, with time series of all flow quantities showing a strong component at the frequency of the GS mode (further details are presented in the discussion). Thus, we are not able to define a critical Reynolds number for transition for this flow, and cannot compare its amplitude to the ZS flow in terms of $(R - R_M)$. If we measure the temporal variation in energy (simply defined as the difference divided by the sum of the extrema in the total energy), the variation for the GS(4, 4) mode is 6.4%, while for the ZS(6, 6) mode it is 5.8%. The latter is at an R about 20% above R_M , suggesting that the GS mode is in a comparable range. However, this measure of the modulation amplitude hides some significant differences between the two types of

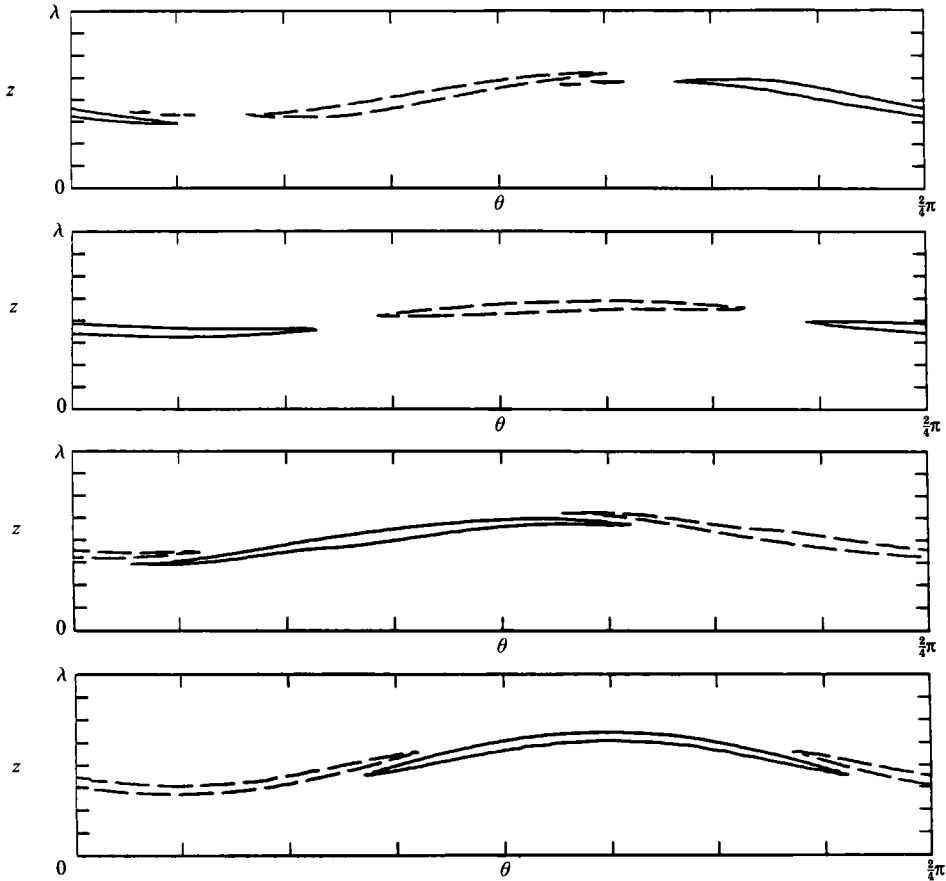


FIGURE 7. Contours of constant azimuthal vorticity for the quasi-periodic piece of the GS mode in figure 6, plotted in the (θ, z) -plane at four equally spaced times. The contour values ± 0.6 are plotted, inside this contour the vorticity increases, and outside drops rapidly to zero.

flow. The distribution of energy variation over axisymmetric versus non-axisymmetric modes is more revealing, since the flattening of the outflow contour observed in GS flow is correlated with a local surge in the axisymmetric fraction of the total energy. For GS flow, the fraction of the energy in the axisymmetric modes varies between 34% and 77% for the axial component of the flow, the radial component varies between 47% and 86%, and the azimuthal component between 87% and 94% (the latter variation is small because v_θ is dominated by the non-fluctuating axisymmetric flow). In contrast, for the ZS(6, 6) flow the variations are: axial, 76–81%; radial, 88–90%; and azimuthal 94–95%. Thus, while the fluctuation in total energy for the two modes is comparable, the distribution of energy over the axisymmetric and non-axisymmetric components of the flow is very different; hence, the amplitude of the quasi-periodic flow depends on the quantity used to measure it.

A more direct measure of the amplitude of the disturbance is in terms of the relative strength of the quasi-periodic vorticity. If we compare the maximum over θ and z of $\hat{\mathbf{e}}_\theta \cdot \nabla \times \mathbf{v}_{qp}$ at fixed r and t , normalized by the strength of ω_θ in the underlying wave, we find that the GS mode is on the order of twice as strong as the ZS mode. The temporal variation in the vorticity is also much larger for GS flows. The disparity in drift speeds of the two flows reflects a different relation between the

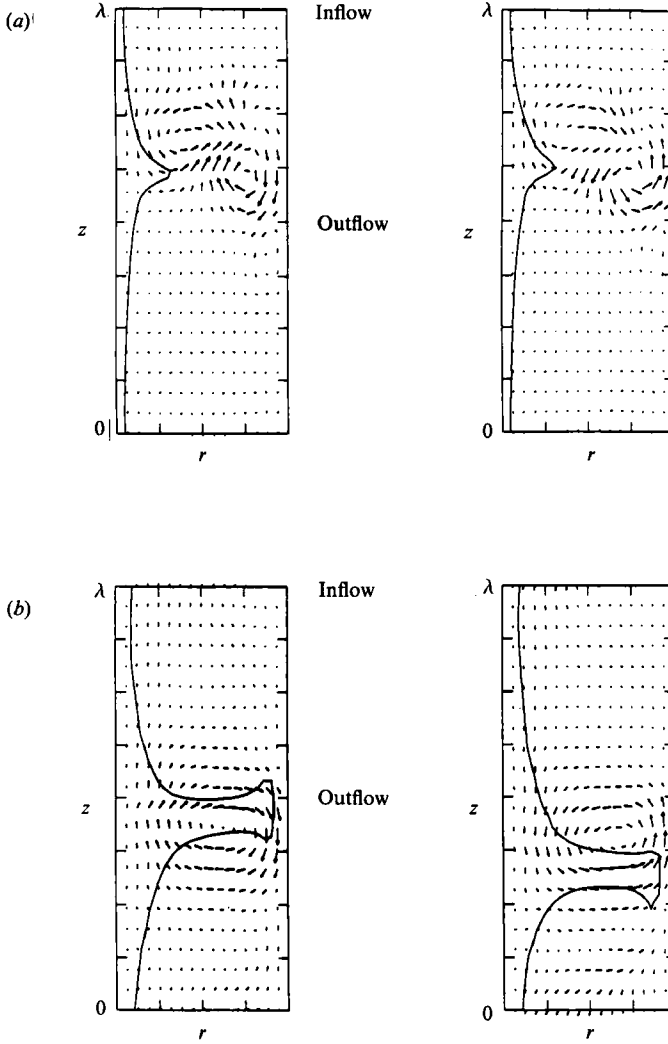


FIGURE 8. Projection of the quasi-periodic velocity field onto an (r, z) -plane at two equally spaced times in the modulation period, for (a) the ZS mode in figure 1 and (b) the GS mode in figure 6. These are overlaid with the contour $v_\theta = rc_d$, on which the azimuthal velocity is equal to the drift speed of the quasi-periodic mode.

location of the quasi-periodic vorticity and its co-moving surface, the contour on which the total azimuthal velocity (relative to the c_1 -frame) is equal to c_d . In figures 8(a) and 8(b) we compare the ZS(4, 12) and the GS(4, 4) modes. The quasi-periodic velocity is projected onto a fixed (r, z) -plane and overlaid with the contour on which $v_\theta = rc_d$. Both flows are shown at two times: t and $t + \frac{1}{2}T_M$. For the GS flow in figure 8(b) the c_d -surface passes near the centres of the vortices, which sit in regions of large shear, whereas for the ZS flow in figure 8(a) the quasi-periodic vorticity is concentrated near the tip of the outflow jet, outside the region of largest axial shear. We remind the reader that the azimuthal velocity of the fluid is largest at the left-hand boundary, and decreases outward. The ZS vortex moves faster than the surrounding fluid, while the GS vortex moves at approximately the local v_θ .

In figure 9 we illustrate the relation between the axial location of the quasi-

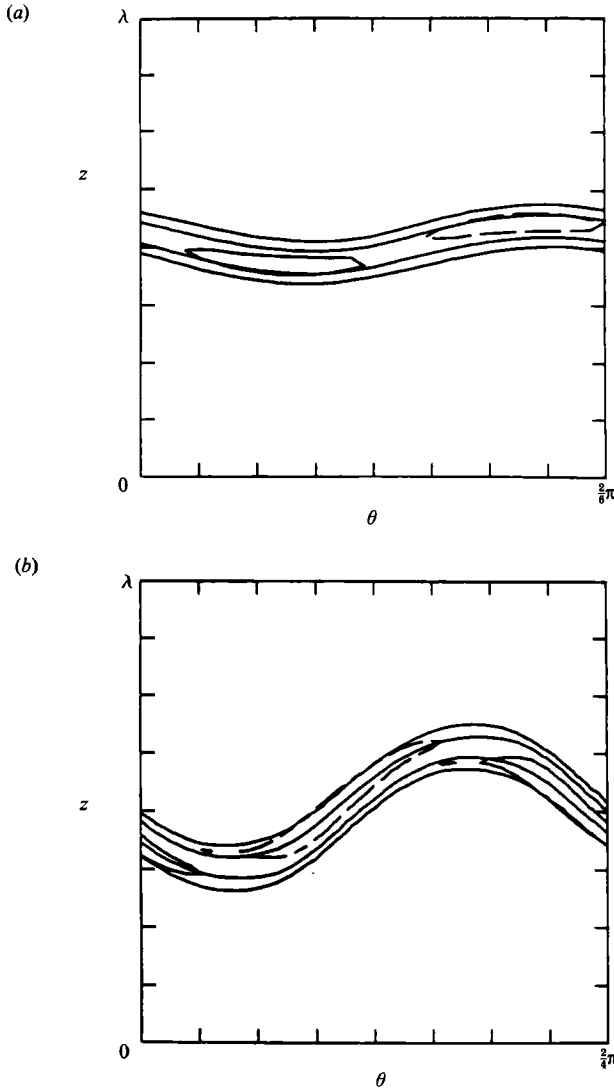


FIGURE 9. The contours of v_θ defining the outflow in the (θ, z) -plane are plotted next to the quasi-periodic vorticity at fixed t for (a) the ZS flow and (b) the GS flow in figure 8.

periodic θ -vorticity and the outflow as defined by the maximal azimuthal velocity. Contours of v_θ at the outflow, in the (θ, z) -plane at mid-gap, are overlaid with the solid or dashed contour defining the quasi-periodic disturbance (as in figures 4 and 7). The ZS modes sit on the flat plateau at the peak of the jet, while the GS modes are centred at the regions of large axial gradient in v_θ . This suggests that the two modes may result from instability of different features of the outflow, with the ZS likely to be associated with the radial outflow, and the GS modes with the axial shear in v_θ .

We have computed a GS modulated wave for only one set of parameter values. The data presented in Gorman & Swinney (1982) indicate that these modes occur, for a variety of azimuthal wavenumbers, in the Reynolds number range $9R_c \leq R \leq 20R_c$. All the flows in that paper were for $\lambda \leq 2.5$. King (1983) stated that for $\lambda \leq 3.0$ the transition to modulated waves takes place at a lower value of R near $7R_c$, although no data on the modulated flow itself was reported. Ross & Hussain (1987) studied the

aspect ratio dependence of the onset of modulation, but did not report the axial wavelengths of their flows. To our knowledge, no other systematic study of the axial wavelength dependence of the transition to quasi-periodic flow has been done. We have computed flows for $\lambda = 3$ and $s = 4$ and 6 , up to $R = 10R_c$, and find no evidence in the time series of the presence of a GS type of modulation. In contrast, for $\lambda = 2.5$, even though the GS mode is not a stable equilibrium until $R \approx 10R_c$, it is evident in our solutions as a decaying transient for R as low as $8R_c$. It thus seems possible that the transitions to quasi-periodicity for $\lambda \geq 3$, occurring at characteristically low R , correspond to ZS modes, and that there may be a critical value of λ above which one no longer finds GS modes.

4. Mechanism of instability

In the previous section we demonstrated that the spatial character and temporal behaviour of modulated waves are intimately connected to the outflow jet of the underlying wave. In this section we will review in more detail the properties of TVF and WVF, and show that the spatial structure of both these flows as a function of R is also determined by the outflow jet. We will argue that the rotating wave and modulated wave flows arise owing to instability of the outflow, and have many features in common. This reduces the complications inherent in understanding the full three-dimensional, time-dependent problem, although not to the point where we are able to claim that the instabilities map on to a simple two-dimensional paradigm. In our discussion of WVF, we shall refer to the axisymmetric or ‘mean’ component of the flow, and the ‘disturbance’, which is defined for WVF as the total minus the mean component. This is different from our usage of ‘mean’ and ‘disturbance’ with respect to modulated waves, however the appropriate definitions should be clear from the context.

4.1. TVF

First we shall argue that the centrifugal instability, beyond the primary transition to TVF, is important only in maintaining the basic vortical structure. As is well known, the transition from circular Couette flow to Taylor vortices can be understood in terms of Rayleigh’s criterion, which states that the inviscid flow is linearly unstable if energy is liberated when two fluid rings of equal mass at r and $r+dr$ are exchanged while conserving angular momentum. In particular, this condition is met if the mean angular momentum $L(r)$ decreases outwards, as it does for any positive value of Ω when the outer cylinder is fixed. For finite viscosity, work is done in the exchange, hence $L(r)$ may have a finite gradient before the flow goes unstable. Taylor vortices mix the fluid in the interior of the flow, flattening the profile of $L(r)$, which stabilizes the flow (see Marcus 1984*b* for a plot of $L(r)$). Numerically, we find that the profiles of $L(r)$ for WVF and MWV are almost identical to $L(r)$ for the unstable TVF at the same R . Beyond $R \sim 6R_c$, this profile is very flat in the interior of the flow, and changes only in the boundary layers which become slightly thinner as R is increased further. The wave and modulated wave disturbances always exist outside the radial boundary layers and have minimal effect on the transport of angular momentum. Experimentally (when the outer cylinder is held fixed) the Taylor vortex structure persists well into the regime where the flow is chaotic. Numerically we find that if non-axisymmetric modes are suppressed, Taylor vortex flow is a steady equilibrium solution up to at least $R = 12R_c$ (for $\lambda = 2.5$ and $\lambda = 3$). The flow is dominated by the outflow jet, which is driven directly by the centrifugal force, and which tends to throw fluid outward from the spinning inner

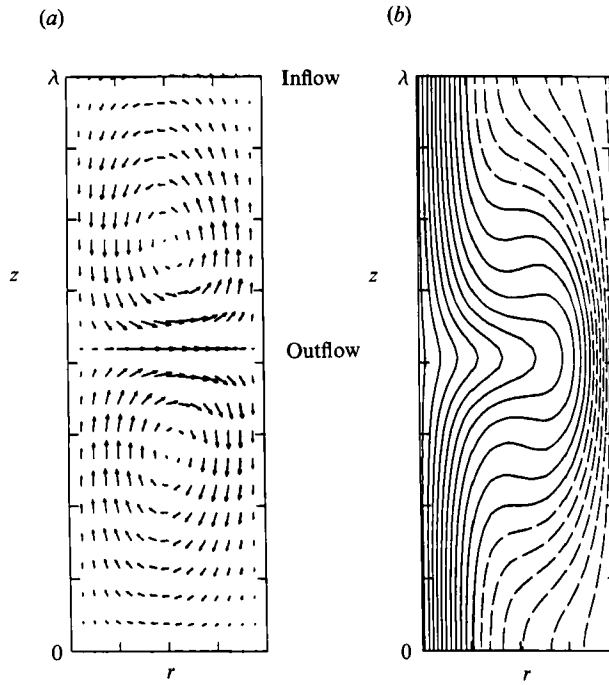


FIGURE 10. Taylor vortex flow for $\lambda = 3$ at $R = 2.1R_c$. (a) The total velocity field is projected onto an (r, z) -plane with the inner cylinder on the left. (b) Contours of constant v_θ are plotted in the same (r, z) -plane.

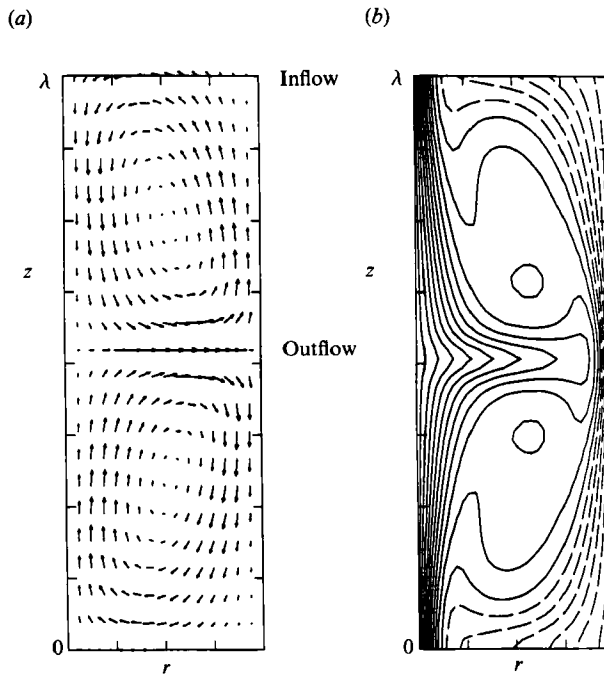


FIGURE 11. Taylor vortex flow for $\lambda = 3$ at $R = 6.5R_c$. (a) The total velocity field is projected onto an (r, z) -plane with the inner cylinder on the left. (b) Contours of $v_\theta = \text{constant}$ are plotted in the same (r, z) -plane.

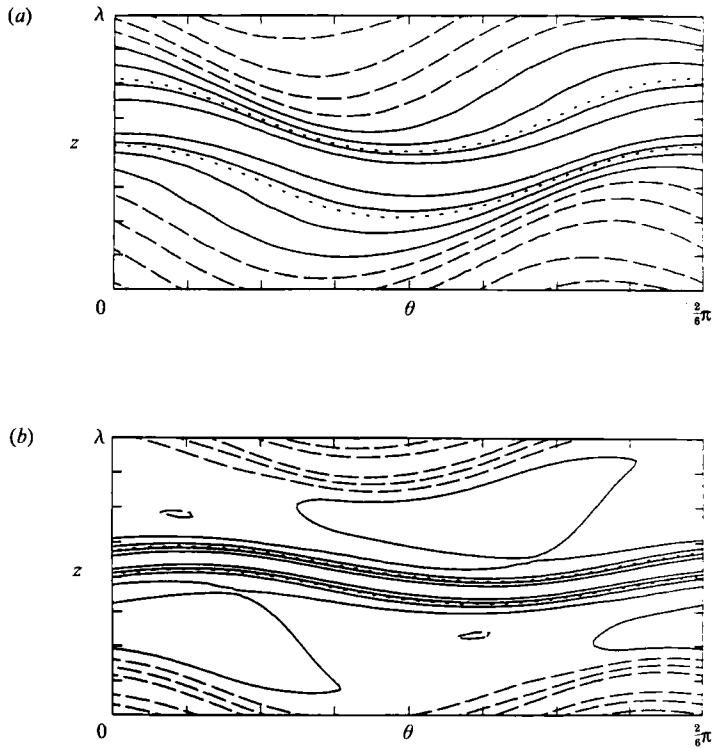


FIGURE 12. Contours of constant v_θ in the (θ, z) -plane at mid-gap for $\lambda = 3$, $s = 6$, at (a) $R = 2.1R_c$ (contour interval = 0.07) and (b) $R = 6.5R_c$ (contour interval = 0.06). The outflow jet is defined by the contour of maximum v_θ . The width of the outflow, defined as the full width at half-maximum of v_θ in this plane, is shown by the short-dashed contour.

cylinder. The inflow jet is driven by the outflow, consequently is broader, weaker, and of secondary importance in the dynamics. The evidence therefore suggests that the basic TVF structure is adequate to neutralize the centrifugal instability, and that subsequent transitions are due to the sharp features that develop at the outflow as R is increased.

We illustrate the structure of the outflow jet, particularly the coupling of v_r and v_θ , using TVF (the important features are not specific to this case). In figure 10 we plot a projection of the velocity field of (unstable) TVF for $\lambda = 3$, $R = 2.1R_c$ onto an (r, z) -plane and, in the same plane, contours of the azimuthal velocity v_θ . With the proper choice of $z = 0$, Taylor vortex flow has shift-and-reflect symmetry, so that the extremal radial and azimuthal velocities occur at $z = 0$ and $\frac{1}{2}\lambda$. This figure demonstrates the co-dependence of the velocities v_r and v_θ on the axial coordinate, as the radial outflow effectively pushes the contours of fast-moving fluid towards the outer cylinder. With increasing R , the axial gradients in v_r and v_θ become sharper, as both the radial and azimuthal jets narrow. This is clearly seen in figure 11, which shows the same projections as in figure 10 for the flow with $R = 6.5R_c$. Note that in our dimensionless units the magnitudes of the velocities remain roughly constant with R . Below we will show that the width of the jet, defined here as the full width at half-maximum of the azimuthal velocity at mid-gap, scales as $(R/R_c)^{-1}$.

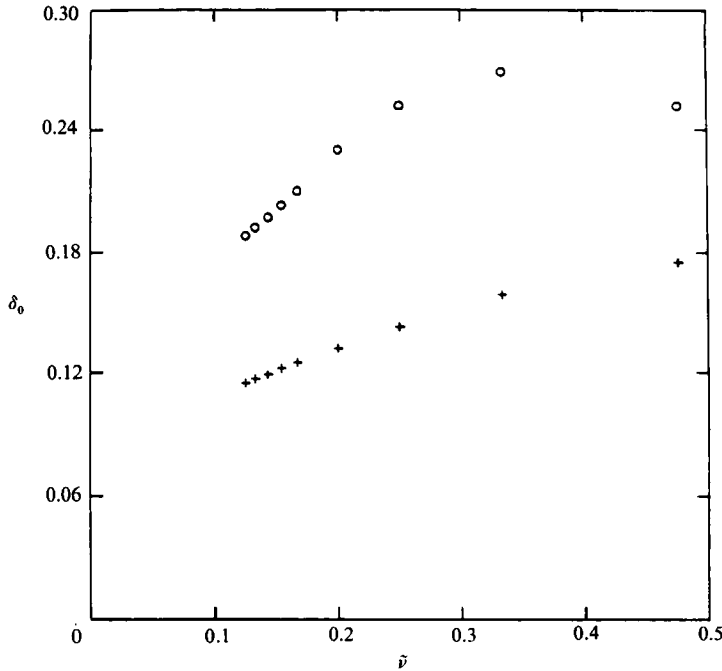


FIGURE 13. Mean outflow jet width δ_0 vs. $\tilde{\nu} \equiv (R/R_c)^{-1}$ for WVF and time-averaged MWV with $s = 6$ (+) and TVF (\circ) for $\lambda = 3$. See (11) for a definition of δ_0 .

4.2. WVF

For all values of s the outflow jet narrows with increasing R . We have found this to be true for TVF, WVF and MWV flows. For WVF, the narrowing is accompanied by an increased localization of the wave disturbance at the outflow, as is illustrated in the next three figures. In figure 12, contours of v_θ are plotted for WVF with $\lambda = 3$, $m_1 = 6$, at $R = 2.1R_c$ and $R = 6.5R_c$. In this projection, the outflow is defined as the contour of maximum v_θ . The extent of the deformation of the outflow in the axial direction decreases somewhat with R , but far more apparent is the decrease in the width of the jet and the consequent large increase in the axial gradients.

We measure the outflow jet width as follows: let $z_m(\theta)$ be the axial location as a function of θ where the azimuthal velocity at mid-gap is a maximum, and $z_{h1,2}(\theta)$ be the two locations where it is at half maximum:

$$v_\theta(\tfrac{1}{2}(a+b), \theta, z_{h1,2}) = \tfrac{1}{2}v_\theta(\tfrac{1}{2}(a+b), \theta, z_m). \quad (9)$$

The contours $z_{h1,2}(\theta)$ are highlighted in figure 12. Define the function $W(\theta)$ as

$$W(\theta) = |z_{h2}(\theta) - z_{h1}(\theta)|. \quad (10)$$

We define the outflow jet width as the average of $W(\theta)$ over θ ;

$$\delta_0 = \int_0^{2\pi} W(\theta) \frac{d\theta}{2\pi}. \quad (11)$$

As can be seen from figure 12, $W(\theta)$ is approximately independent of θ , being roughly equal to δ_0 everywhere. This is true of TVF, WVF and MWV, independent of s , for $R \gtrsim 6R_c$. In figure 13 we plot δ_0 as a function of the dimensionless viscosity $\tilde{\nu} \equiv R_c/R$, for (unstable) TVF with $s = 6$, and WVF, and time-averaged MWV. For $\tilde{\nu} < 0.25$ the width of the jet in all types of flow decreases approximately linearly with $\tilde{\nu}$. The inflow jet width is also linearly dependent on $\tilde{\nu}$.

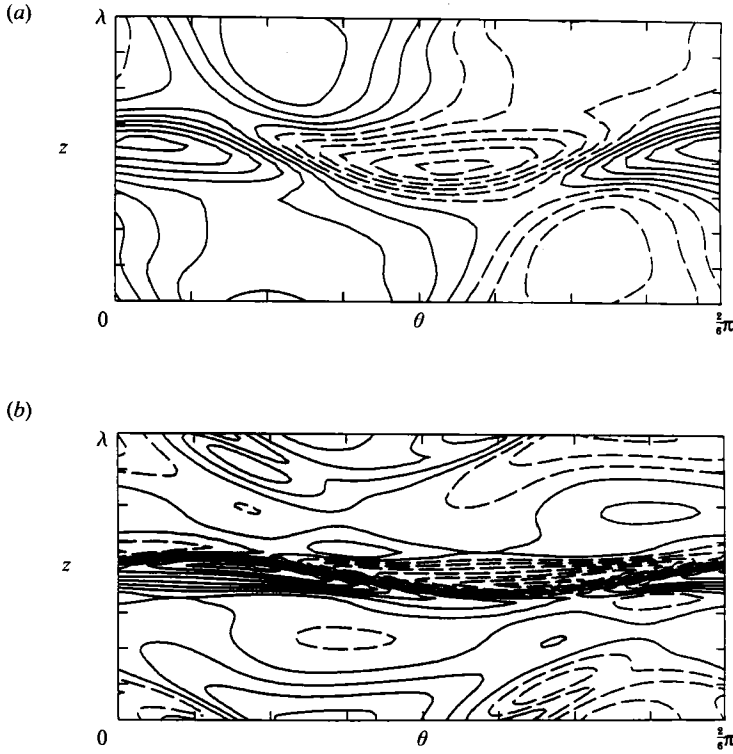


FIGURE 14. The non-axisymmetric component of ω_θ in the (θ, z) -plane at mid-gap for wavy vortex flow at (a) $R = 2.1R_c$ and (b) $R = 6.5R_c$, showing the vortex pairs which constitute the wave disturbance. The contour interval is 0.12.

In figure 14 we plot the non-axisymmetric component of ω_θ in the (θ, z) -plane at mid-gap for WVF at $R = 2.1R_c$ and $R = 6.5R_c$. The wave disturbance consists of regions where the vorticity is concentrated into pairs of opposite sign, one pair at the inflow and one pair at the outflow. This structure can be explained as follows: for WVF, the axisymmetric component of the flow has essentially the same structure as TVF, consisting of two tubes of azimuthal vorticity wrapped around the cylinder. For TVF, the axial reflection symmetry implies that $\omega_\theta(r, z) = -\omega_\theta(r, -z)$, so the inflow and outflow boundaries define contours at $z = 0$ and $z = \frac{1}{2}\lambda$ on which $\omega_\theta = 0$, with negative vorticity in the vortex above the outflow and positive below. For WVF, the wave deflects these contours, with the non-axisymmetric disturbance equal to the difference between the shifted and unshifted vortex boundaries. Where the contour is deflected upward there is a net surplus of vorticity relative to the mean flow, and where it is deflected downward a net deficit. The WVF disturbance flow is shift-and-reflect symmetric so $\omega_\theta(r, \theta, z) = -\omega_\theta(r, \theta + \pi/s, -z)$ and the upward and downward deflections of the contour are equal and opposite. Thus, the non-axisymmetric component of WVF consists of two pairs of compact regions of azimuthal vorticity, one at the outflow and one at the inflow. The more compact vortices are at the outflow, where the jet is stronger. At higher R , the localization of the non-axisymmetric flow to the inflow and the outflow regions is quite pronounced. In our scaled units, the maximum value of ω_θ remains approximately constant with R (it is 0.85 at $2.1R_c$ and 0.91 at $6.5R_c$). At low R the disturbance vorticity is about 60% stronger at the outflow than it is at the inflow, and this disparity increases to nearly

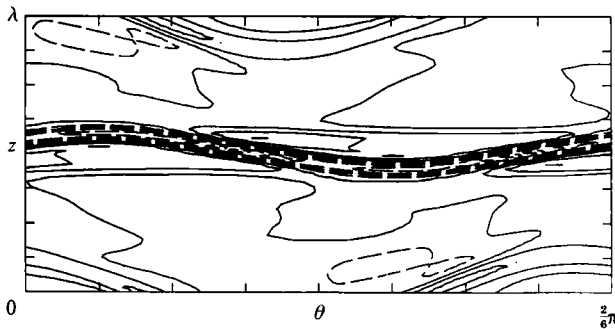


FIGURE 15. Plot of the non-axisymmetric piece of the nonlinear term, $\hat{\mathbf{e}}_\theta \cdot ((\mathbf{v} \cdot \nabla) \mathbf{v})$ in the (θ, z) -plane at mid-gap for WVF with $\lambda = 3$, $s = 6$, $R = 6.5R_c$. Contour interval is 0.01.

300% at high R , reflecting the growing asymmetry in the inflow and outflow strengths, and the relative unimportance of the inflow. Comparison of figures 12 and 14 shows that the non-axisymmetric ω_θ is localized to within $\pm \delta_0$ of the outflow.

The scaling $\delta_0 \sim (R/R_c)^{-1}$ can be derived from dominant balance in the equation for v_θ . Computations of Taylor–Couette flows show that the R -dependence of the energy and enstrophy associated with the time-dependent component of the flow is very weak. Thus, in what follows, we take the magnitudes of the velocity and vorticity to be constant with R . The azimuthal derivatives are small and the flow in the rotating frame is steady. Outside the boundary layers, the radial derivatives near the outflow are small compared to the axial derivatives, so the time-dependent Navier–Stokes equation for v_θ reduces to

$$(v_r \partial_r + v_z \partial_z) v_\theta \sim \nu \partial_{zz} v_\theta. \quad (12)$$

We include both the radial and azimuthal components of the nonlinear term because near the outflow v_z may be small. For WVF and MWV in the range of interest the two nonlinear terms are of the same order. Thus, setting axial derivatives $\sim 1/\delta_0$, the outflow width scales as

$$\delta_0 \sim \nu \times \text{constant}. \quad (13)$$

The constant depends on the parameters s and λ , but the scaling with R is independent of both the axial and azimuthal wavelength.

We hypothesize that the narrowing of the outflow (and inflow) jets produces the localization of the wave disturbance in the following manner: energy is input to the system through the torque at the inner cylinder, which drives only the axisymmetric, axially symmetric component of v_θ . Most of this energy is dissipated directly in the boundary layers, with the remainder driving the rest of the flow. In particular, the non-axisymmetric modes derive their energy from the mean flow through the nonlinear term in the Navier–Stokes equations. The width of the outflow jet is a measure of the steepness of the axial gradients in that region of the flow, and thus of the strength of nonlinear interactions there. It is reasonable that the non-axisymmetric disturbance (which is also the time-dependent component of the flow in the inertial frame) is strongest where gradients are large and the nonlinear transfer of energy is most effective. The radial jets produce these gradients in v_θ by advection of the azimuthal flow. To support this argument, we plot in figure 15 the non-axisymmetric component of $\hat{\mathbf{e}}_\theta \cdot ((\mathbf{v} \cdot \nabla) \mathbf{v})$ in the (θ, z) -plane at mid-gap for WVF at $R = 6.5R_c$. This term represents the transfer of energy into the non-axisymmetric modes of the Navier–Stokes equations, and is clearly peaked at the jets (particularly the outflow).

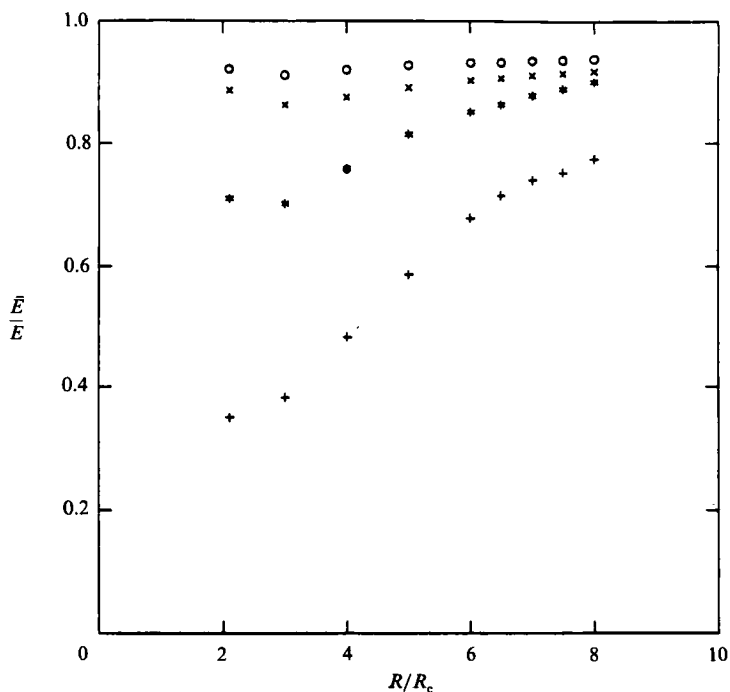


FIGURE 16. Ratio of the energy in the axisymmetric modes of the flow to the total energy, as a function of R , for flows with $\lambda = 3$ and $s = 6$. The radial (*), azimuthal (x) and axial (+) energies, and the total (O), are plotted. See (14) and (15) for definitions of the energies.

Overall, as R increases the WVF becomes more like TVF, i.e. more axisymmetric. This can be quantified in a global way by considering the fraction of energy that is in the axisymmetric component of the flow. For the radial component, we define the total energy as

$$E_r = \frac{1}{2\lambda} \int_a^b \int_0^{2\pi} \int_0^\lambda |v_r|^2 r dr d\theta dz, \quad (14)$$

and the axisymmetric energy as

$$\bar{E}_r = \frac{1}{4\pi\lambda} \int_a^b \int_0^\lambda \left| \int_0^{2\pi} v_r d\theta \right|^2 r dr dz, \quad (15)$$

and similarly for the θ - and z -components. (For the θ -component, we remove the contribution of the circular Couette flow from the total v_θ .) The total (axisymmetric) energy of the flow is just $E = E_r + E_\theta + E_z$ ($\bar{E} = \bar{E}_r + \bar{E}_\theta + \bar{E}_z$). We plot the ratio \bar{E}_i/E_i for each component of the velocity separately, and for the total \bar{E}/E , in figure 16 for $\lambda = 3$, $s = 6$ and $2.1R_c \leq R \leq 8R_c$. Also included in the plot are time-averaged values for MWV states with $R > 7R_c$. At low Reynolds number, as the wave amplitude grows with R , the ratio \bar{E}/E decreases. However, beyond $R \sim 4R_c$ the relative magnitude of the axisymmetric energy begins to increase, and levels off to an approximately constant value (within a few per cent) near $R = 6R_c$; hence, the flow becomes more axisymmetric (the wave amplitude decreases) at larger R .

4.3. Outflow jet instability

The evidence suggests that all the instabilities which occur in this flow after the transition to TVF are due to the outflow. Jones (1981, 1985) argued that the transition from TVF to WVF results from an Orr–Sommerfeld instability of the axial shear in v_θ . Marcus (1984*b*) proposed an alternative scenario in which the WVF arises

from an instability of the radial outflow, supported by the fact that the WVF eigenmode consists of vortices in the (θ, z) -plane, with centres located exactly at the outflow and inflow jets. If the instability were due to the shear, these vortices should be centred at the inflexion points of v_θ , which are located half-way between the inflow and outflow boundaries. In both scenarios the important features are the jets between adjacent Taylor vortices, in particular the outflow jet where both the velocities (v_r and v_θ) and the axial shear are greatest. The Navier–Stokes equations linearized around Taylor vortex flow are autonomous in θ and t , so generically any mode which breaks these symmetries will have the mathematical form of a rotating wave (Rand 1982). Physically, any mode that is localized near the outflow is subjected to the strong ambient azimuthal velocity; hence it is not surprising to find instabilities in the form of azimuthally travelling waves.

The spatial localization of the Floquet eigenmodes of WVF implies that the transition to MWV is also due to instability of the outflow. The quasi-periodic disturbance results in increased axial flow across the radial and azimuthal jets. The strength of each jet (for both ZS and GS flows) oscillates in time around its mean value, which is likely to be lower than for the unstable WVF at the same R (we have not proved this, since the exact unstable WVF is unavailable for comparison). The transition from WVF to MWV is similar in many ways to the transition from TVF to WVF, and we believe that the former is due to instability of the approximately axisymmetric outflow jet. For the transition from WVF to MWV, the quasi-periodic flow has a lower ratio of \bar{E}/E , indicating that the disturbance draws energy primarily from the axisymmetric modes. The spatial structure and dynamical behaviour of both the non-axisymmetric wave in WVF and the quasi-periodic disturbances in MWV are dominated by the advection of coherent, three-dimensional vortices by the ambient azimuthal flow. They differ in that the WVF disturbance has significant amplitude at the inflow jet, whereas the quasi-periodic mode does not. However, we can attribute this disparity to the fact that when TVF becomes unstable to WVF the inflow and outflow jets are almost symmetric, whereas at higher R where the quasi-periodic instability occurs they are highly asymmetric. Both instabilities of the outflow come in with an azimuthal phase dependence of the form $e^{im(\theta-ct)}$, multiplying a function with the same space–time symmetry as the underlying flow. For the transition to MWV, the primary effect of the initial rotating wave is to prohibit the existence of a preferred frame in which the modulation is steady, so that the total flow must be quasi-periodic. Equivalently, the θ dependence of the underlying WVF prevents the drifting modulation from being a true rotating wave in any frame, but is otherwise not important.

5. Discussion

5.1. Summary

We have solved the Navier–Stokes equations numerically for a number of modulated wavy flows (MWV), using the detailed information about the flow to associate a simple physical process with the modulation. In the rotating frame the quasi-periodic disturbance (defined as the total flow minus the time-averaged, steady-state piece) appears as a set of compact, coherent vortices confined almost entirely to the outflow jet region. They are advected (with some distortion) in the θ -direction along the outflow between adjacent Taylor vortices, with the frequency of modulation directly related to the mean drift speed. The azimuthal wavelength of the disturbance field determines the second wavenumber (m_2). We have argued that, at high Reynolds number, the modulation arises as an instability of the essentially axisymmetric

vortex outflow jet. This picture of modulated wave holds for the distinct ZS and GS branches of MWV solutions. Experimental observations have confirmed that both modes exist. We note that these solutions do not constitute an exhaustive study of quasi-periodic states in the Taylor–Couette system.

The picture of a fixed sequence of bifurcations occurring in Taylor–Couette flow at this radius ratio with increasing R , known from experiments to be complicated by changes of axial and azimuthal wavelength, has been found in our work to be misleading in a more fundamental way: there are bifurcation sequences that do not follow this scenario even when ‘end effects’ are eliminated and the axial and azimuthal wavelengths are forced to remain fixed. In particular we note that: (i) while we have seen direct bifurcations from WVF to ZS flows, we have found no indication of a direct bifurcation from WVF to a GS flow. A careful review of the published experimental work (Gollub & Swinney 1975; Gorman & Swinney 1982; King 1983; Brandstater & Swinney 1987) shows that there is in fact no experimental evidence of such a transition. (Instead, the usual procedure is to reach the desired state from a chaotic flow at higher R by reducing the inner cylinder speed.) Numerically, we have found a transition from a ZS mode, through an aperiodic flow, to a GS mode as R increases. These transitions have since been seen in the laboratory (Coughlin *et al.* 1991). Thus, not all MWV states are bifurcations from WVF, and the direction of bifurcation with increasing R is not always to a state with lower symmetry; (ii) there is, implicit in the main sequence scenario, an assumption that a single, generic bifurcation to chaos occurs in this system. Our numerical results show that this is not the case. We have found a chaotic flow which appears to result from mode competition between ZS and GS modes (described further below), and in other work, examples of both intermittency and a Feigenbaum period-doubling cascade (Coughlin 1990; Coughlin & Marcus 1992*b*).

5.2. The transition to chaos

Quasi-periodic modes in the Taylor–Couette system have historically been of interest because of experiments on the transition from GS modes to chaos (Gollub & Swinney 1975). Quantitative laboratory measurements have shown that the chaotic state is low-dimensional, and that the transition is continuous and non-hysteretic (Fenstermacher *et al.* 1979; Brandstater & Swinney 1987). Because the MWV state is temporally periodic relative to the correct rotating frame, the experiments imply that there is a direct bifurcation from a limit cycle to a chaotic attractor. This type of bifurcation is not understood, in the sense that no simple mathematical models exhibiting this behaviour are known.

Experimentally, the visual signature of the onset of chaos is the appearance of aperiodic, small-scale structure in the outflow jet region, which eventually spreads to the rest of the flow as R is further increased (Gorman, Reith & Swinney 1980). We hypothesize that there are a number of distinct linear Floquet modes associated with instability of the outflow jet, each of which, when it becomes active (i.e. acquires positive growth rate) contributes a new dynamical degree of freedom to the system. In particular, the transition from GS flow to chaos may be mediated by the introduction of another unstable Floquet mode.† Subsequently, several things may

† This conjecture is supported by recent work of Vastano & Moser (1991), who calculated Lyapunov exponents and the related linear eigenfunctions for the chaotic flow, showing that the latter consist of concentrations of vorticity at the outflow jet, similar to the quasi-periodic Floquet modes presented in this paper.

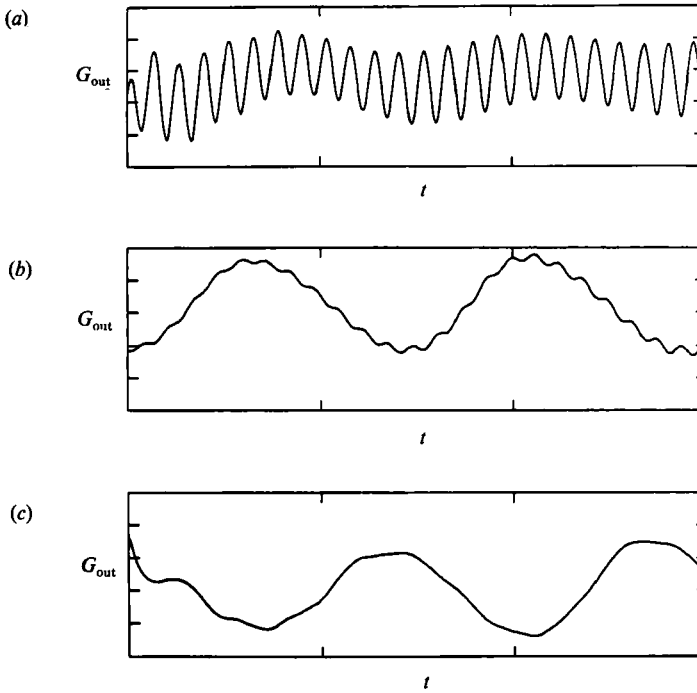


FIGURE 17. Time series of the torque at the outer cylinder G_{out} for the flow with $\lambda = 2.5$ at three different Reynolds numbers. The length of the time series shown is approximately 11 inner cylinder periods. (a) At $R = 8.7R_c$ the flow converges to a ZS(4, 12) mode as the GS(4, 4) transient decays. (b) At $R = 9.25R_c$ both the GS and the ZS modes are present with positive growth rate for as long as the computation was run (over 50 inner cylinder periods). (c) At $R = 9.8R_c$ the flow converges to the GS(4, 4) equilibrium with evidence of the ZS mode in the initial transients.

happen. A stable two-torus (relative to the c_1 -frame) may exist over some (possibly very small) range of R , which can then follow the ‘quasi-periodic’ route to chaos, (Feigenbaum, Kadanoff & Shenker 1982). Or, there may be aperiodicity over a range of R , owing to a type of mode competition, as may happen near a bi-critical point (Ciliberto & Gollub 1985). Either scenario leads to purely temporal chaos, which can have perfect axial and azimuthal periodicity, since the Floquet modes are not spatially disordered.

Additional support for the idea that chaos is associated with several active Floquet modes comes from our numerical discovery that ZS and GS Floquet modes coexist over the same region of R and interact to produce an apparently aperiodic flow. For the flow with $\lambda = 2.5$, $s = 4$ the following sequence occurs: at $R = 8.7R_c$ a stable ZS(4, 12) equilibrium exists, and the transients in the initial-value simulations are dominated by a mode with the frequency of the GS(4, 4) mode. At $R = 9.8R_c$ this GS mode is stable, and the decaying transients leading to this equilibrium show evidence of the high-frequency ZS(4, 12) mode. At $R = 9.0R_c$ and $R = 9.25R_c$, time series show that both the ZS and GS modes are present with positive growth rate. The flow at this R is aperiodic over the entire integration time (about 40 inner cylinder periods). We show an example of time series at these three Reynolds numbers in figure 17. Both modes are evidently Floquet modes of the underlying WVF, with positive or negative growth rate at values of R consistent with the observed equilibria. Figure 18 shows schematically the growth rates as a function of R . The existence of this sequence of states has been experimentally confirmed (Coughlin *et al.* 1991), and will

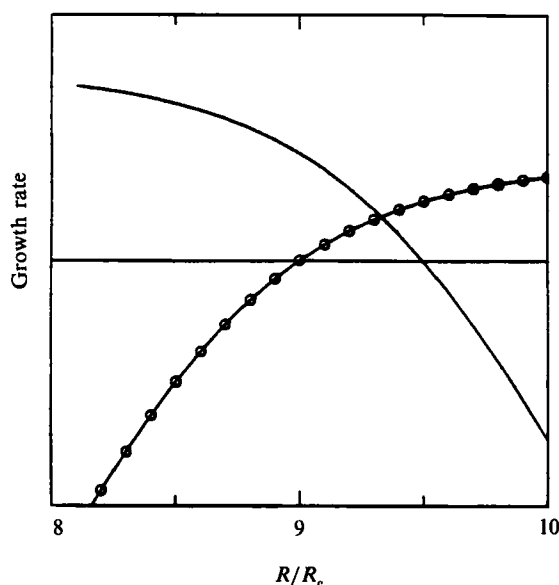


FIGURE 18. Sketch of the hypothetical growth rate of the ZS (solid) and GS (solid with circles). Floquet modes *vs.* R/R_c . For $R \lesssim 9.0R_c$, only the ZS mode has positive growth rate and it is a stable equilibrium. For $R \gtrsim 9.6R_c$, the GS mode has positive growth rate and is stable. For $9.0R_c \lesssim R \lesssim 9.6R_c$, both modes have positive growth rate and the flow may be chaotic. The vertical scale is arbitrary.

be used in future work to investigate the transition to chaos, both with full simulation and low-dimensional spectral truncations of the Navier–Stokes equations.

We thank Harry L. Swinney and R. Tagg for interesting and helpful discussions of the experimental work. This work was supported in part by National Science Foundation Grant CTS-89-06343. The numerical computations were done at the San Diego Supercomputer Center.

REFERENCES

- ABRAHAM, N. B., GOLLUB, J. P. & SWINNEY, H. L. 1984 Testing nonlinear dynamics. *Physica* **11D**, 252–264.
- ANDERECK, C. D., LIU, S. S. & SWINNEY, H. L. 1986 Flow regimes in a circular Couette system with independently rotating cylinders. *J. Fluid Mech.* **164**, 155–183.
- BRANDSTATER, A., SWIFT, J., SWINNEY, H. L., WOLF, A. & FARMER, J. D. & JEN, E. & CRUTCHFIELD, P. 1983 Low-dimensional chaos in a hydrodynamic system. *Phys. Rev. Lett.* **51**, 1442–1445.
- BRANDSTATER, A. & SWINNEY, H. L. 1987 Strange attractors in weakly turbulent Couette–Taylor flow. *Phys. Rev. A* **35**, 2207–2220.
- CILIBERTO, S. & GOLLUB, J. P. 1985 Chaotic mode competition in parametrically forced surface waves. *J. Fluid Mech.* **158**, 381–398.
- COLE, J. A. 1976 Taylor-vortex instability and annulus-length effects. *J. Fluid Mech.* **75**, 1–15.
- COLES, D. 1965 Transition in circular Couette flow. *J. Fluid Mech.* **21**, 385.
- COUGHLIN, K. 1990 Quasi-periodic Taylor–Couette flow. Thesis, Physics Department, Harvard University.
- COUGHLIN, K. T. & MARCUS, P. S. 1992*a* Modulated waves in Taylor–Couette flow. Part 1. Analysis. *J. Fluid Mech.* **234**, 1–18.
- COUGHLIN, K. T. & MARCUS, P. S. 1992*b* Period-doubling in a three-dimensional flow. In preparation.

- COUGHLIN, K. T., MARCUS, P. S., TAGG, R. P. & SWINNEY, H. L. 1991 Distinct quasiperiodic modes with like symmetry in a rotating fluid. *Phys. Rev. Lett.* **66**, 1161–1164.
- DINAR, N. & KELLER, H. B. 1985 Computations of Taylor vortex flows using multigrid computation methods. *Cal-Tech Applied Mathematics Report*.
- FASEL, H. & BOOZ, O. 1984 Numerical investigation of supercritical Taylor-vortex flow for a wide gap. *J. Fluid Mech.* **138**, 21–52.
- FEIGENBAUM, M., KADANOFF, L. & SHENKER, S. 1982 *Physica* **5D**, 370.
- FENSTERMACHER, P. R., SWINNEY, H. L. & GOLLUB, J. P. 1979 Dynamical instabilities and the transition to chaotic Taylor vortex flow. *J. Fluid Mech.* **94**, 103–128.
- GOLLUB, J. P. & SWINNEY, H. L. 1975 Onset of turbulence in a rotating fluid. *Phys. Rev. Lett.* **35**, 927–930.
- GOLUBITSKY, M. & STEWART, I. 1986 Symmetry and stability in Taylor–Couette flow. *SIAM J. Math. Anal.* **17**, 249–288.
- GORMAN, M., REITH, L. A. & SWINNEY, H. L. 1980 Modulation patterns, multiple frequencies, and other phenomena in circular Couette flow. *Ann. NY Acad. Sci.* **357**, 10–21.
- GORMAN, M. & SWINNEY, H. L. 1979 Visual observation of the second characteristic mode in a quasiperiodic flow. *Phys. Rev. Lett.* **43**, 1871–1875.
- GORMON, M. & SWINNEY, H. L. 1982 Spatial and temporal characteristics of modulated waves in the circular Couette system. *J. Fluid Mech.* **117**, 123–142.
- JONES, C. A. 1981 Nonlinear Taylor vortices and their stability. *J. Fluid Mech.* **102**, 249–261.
- JONES, C. A. 1985 The transition to wavy Taylor vortices. *J. Fluid Mech.* **157**, 135–162.
- KING, G. P. 1983 Limits of stability and irregular flow patterns in wavy vortex flow. PhD thesis, University of Texas.
- KING, G. P., LI, Y., LEE, W., SWINNEY, H. L. & MARCUS, P. S. 1982 Wave speeds in wavy Taylor vortex flow. *J. Fluid Mech.* **141**, 365–390.
- KING, G. P. & SWINNEY, H. L. 1983 Limits of stability and irregular flow patterns in wavy vortex flow. *Phys. Rev. A* **27**, 1240–1243.
- MARCUS, P. S. 1984*a* Simulation of Taylor–Couette flow. Part 1. Numerical methods and comparison with experiment. *J. Fluid Mech.* **146**, 45–64.
- MARCUS, P. S. 1984*b* Simulation of Taylor–Couette flow. Part 2. Numerical results for wavy-vortex flow with one travelling wave. *J. Fluid Mech.* **146**, 65–113.
- MULLIN, T. 1985 Onset of time dependence in Taylor–Couette flow. *Phys. Rev. A* **31**, 1216–1218.
- MULLIN, T. & BENJAMIN, T. B. 1980 Transition to oscillatory motion in the Taylor experiment. *Nature* **288**, 567–569.
- PARK, K. 1984 Unusual transition in Taylor wavy vortex flow. *Phys. Rev. A* **20**, 3458–3460.
- PARK, K. J., CRAWFORD, G. L. & DONNELLY, R. J. 1981 Determination of transition in Couette flow in finite geometries. *Phys. Rev. Lett.* **47**, 1448.
- RAND, D. 1982 Dynamics and Symmetry. Predictions for modulated waves in rotating fluids. *Arch. Rat. Mech. Anal.* **79**, 1–38.
- ROSS, M. P. & HUSSAIN, A. K. M. F. 1987 Effects of cylinder length on transition to doubly periodic Taylor–Couette flow. *Phys. Fluids* **30**, 607–609.
- SHAW, R. S., ANDERRECK, C. D., REITH, L. A. & SWINNEY, H. L. 1982 Superposition of travelling waves in the circular Couette system. *Phys. Rev. Lett.* **48**, 1172–1175.
- VASTANO, J. A. & MOSER, R. D. 1991 Short-time Lyapunov exponent analysis and the transition to chaos in Taylor–Couette flow. To appear in *J. Fluid Mech.*
- ZHANG, L. & SWINNEY, H. L. 1985 Nonpropagating oscillatory modes in Couette–Taylor flow. *Phys. Rev. A* **31**, 1006–1009.